

Cold Metal Transfer Welding of Dissimilar A6061 Aluminium Alloy-AZ31B Magnesium Alloy: Effect of Heat Input on Microstructure, Residual Stress and Corrosion Behavior

S. Madhavan^{1,2} · M. Kamaraj² · L. Vijayaraghavan¹ · K. Srinivasa Rao³

Received: 5 November 2015 / Accepted: 29 April 2016 / Published online: 24 May 2016
© The Indian Institute of Metals - IIM 2016

Abstract Lap joints of aluminum alloy A6061-T6 and AZ31B magnesium alloy were produced by cold metal transfer welding with Al-5 %Si filler metal. Four heat inputs designated as A (175 J/mm), B (185 J/mm), C (195 J/mm) and D (205 J/mm) were used during the process and the joints made were subjected to analysis of microstructure, mechanical properties and corrosion behaviour. The thickness of the fusion line (diffusion layer) varied from 3 to 12 μm depending on the heat input. It was also found that the joints made using the heat input of 205 J/mm exhibited highest tensile strength of 360 N/mm, least tensile stress in the weld and better pitting corrosion resistance. Electron microscopy study of the weld revealed the presence of β' -Mg₂Si, Al₆Mn and β -Al₃Mg₂ particles. X-ray diffraction study in the weld revealed the formation of γ -Al₁₂Mg₁₇ and β -Al₃Mg₂ phase with Mg₂Si strengthening precipitates. Tensile failure occurred at the fusion line near magnesium.

Keywords Aluminum/magnesium alloy · CMT welding · Microstructure · Mechanical property · Residual stress · Corrosion

1 Introduction

Vehicle weight reduction is a major concern for the automotive industry to enhance fuel efficiency and reduce CO₂ emissions. Aluminium has been used in the car structures and magnesium is mainly used in engine blocks, pump housings and seat frames [1]. The Al–Mg composite structure allows substantial weight reduction and provides design flexibility with extended application in automotive and aerospace manufacturing [2]. Joined parts made of aluminum and magnesium are widely used in places, where high strength and reduced weight are the main concern. However, the welding of Al and Mg alloys has been facing a big challenge due to difference in their thermo-physical and chemical properties [3]. As a potential member for structural and mechanical application, magnesium alloys have been welded by several methods, such as gas tungsten arc welding (GTAW) [4], laser welding [5], laser-GTAW welding [6, 7], friction stir welding [8] and electron beam welding [9]. Al to Mg weldability is poor due to formation of brittle compounds of Mg rich (Mg₁₇Al₁₂) in the weld and they lead to undesirable mechanical strength [10, 11]. Some solid state methods are also being used to reduce the formation of intermetallic phases. They are diffusion bonding [12], electromagnetic pulse welding [13] and resistance welding. The strength of the hybrid joint does not meet the needs of the application and the strength has to be improved further. Laser welding of Mg to Al alloys have been carried out. Microstructural analysis reveals the formation of Mg–Al intermetallic layers leading to degradation of the joining strength at the interface between the two metals [14]. Explosive welding is generally used in bonding of dissimilar materials where the formation of brittle phase is unavoidable. However due to strain hardening, the microstructures become deteriorated and distorted by tremendous force.

✉ S. Madhavan
madhavan.tes@gmail.com

¹ Department of Mechanical Engineering, Indian Institute of Technology Madras, Chennai, Tamil Nadu 600036, India

² Department of Metallurgical and Materials Engineering, Indian Institute of Technology Madras, Chennai, Tamil Nadu 600036, India

³ Department of Metallurgical Engineering, Andhra University, Visakhapatnam 530003, India

Moreover, residual stresses are produced due to difference in linear expansion coefficients [15]. Friction Stir Welding on A6013 over Pure Mg sheet has been carried out. This results in the formation of 23 μm thick intermetallic layer predominantly containing $\text{Al}_{12}\text{Mg}_{17}$ and Al_3Mg_2 phases. The structure and size of solid state joints are restricted because friction stir welding is not suitable due to complexity in shape and size of the component [16].

Four different lap configurations (Mg/Mg, Al/Al, Mg/Al (Mg alloy is the upper sheet) and Al/Mg (Al alloy is the upper sheet) with preheating have been employed to join 6061-T6 aluminium alloy and AZ31B magnesium alloy by friction stir spot welding. It is found that welds with similar metals has the highest tensile strength. Preheating results in bigger nuggets with wider bonding area but presence of $\text{Mg}_{17}\text{Al}_{12}$ intermetallic compound leads to degradation of the joint strength [17]. Control over the heat input is achieved by the cold metal transfer (CMT) process developed by Fronius Company. The CMT process makes use of a simple mechanical assembly for to and fro motion of the wire and helps in metal transfer. Similar welding of Al-Zn alloy has been carried out using Al-5 %Mg filler wire by the CMT process. It is found that CMT provides better joint strength and ductility compared to conventional GMA and GTA welding. It is evident from the microstructures that the primary strengthening precipitate dissolved in the weld metal aids in improving the joint strength [18].

Keeping in mind the above issues, the present work investigates the effect of heat input on the weldability of AZ31B Magnesium alloy and A6061-T6 Aluminium sheets by CMT process. Microstructure of weld zone, diffusion layer or fusion line, tensile strength of the joints, residual stresses and corrosion behavior are analysed. Especially the intermetallic compounds are critically analyzed by scanning electron microscopy (SEM), X-ray diffraction (XRD) and high resolution transmission electron microscopy (HR-TEM).

2 Materials and Methods

2.1 Materials

Aluminium alloy A6061-T6 and magnesium alloy AZ31B with dimensions of $2 \times 40 \times 140$ mm and $3 \times 40 \times$

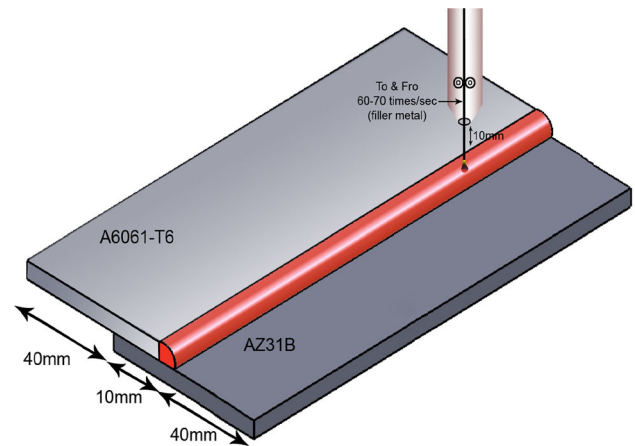


Fig. 1 Schematic of CMT welding of aluminum A6061-T6 and magnesium AZ31B sheets with welding torch and workpiece configuration

140 mm were used. Al-5 %Si filler wire with 1.2 mm diameter was used as filler metal. Nominal chemical compositions of the base metals and the filler are listed in Table 1. The experiments were carried out based on L_9 orthogonal array. For the sake of clarity, process parameters with low, intermediate, medium and high values of heat inputs designated as A, B, C and D respectively were alone reported. Figure 1 shows the schematic of the experimental setup and process.

2.2 Experimental Procedures

The dimensions of the plates were 45 mm \times 130 mm. The oxide film was removed before welding by using wire brush and cleaned with acetone. Lap joints were produced by CMT process with aluminum sheet over the magnesium. Welding parameters used to obtain heat inputs A, B, C and D are shown in Table 2. Shielding gas used in this experiment was commercially pure argon (Purity of 99.9 %), and the gas flow rate was 18 L/min. The heat input was calculated by using an oscilloscope arrangement. A digitized storage oscilloscope was used for recording the current and voltage during the welding. The voltage and current were measured between the workpiece and the welding torch near the contact tip, and stored directly into the oscilloscope. The average value was determined after several similar trails from the stored waveforms. The

Table 1 Chemical composition of Al alloy A6061-T6, Magnesium alloy AZ31B and Al-5 %Si filler (wt%)

Alloys	Al	Fe	Mg	Si	Cr	Ti	Mn	Cu	Zn
A6061-T6	97.4	0.45	0.8	0.6	0.20	0.10	–	0.25	0.2
AZ31B	2.72	–	95.84	0.028	–	0.011	0.29	–	1.11
Al-5 %Si filler	93.6	0.72	–	5.2	–	0.16	–	0.22	0.05

Table 2 Welding parameters used to obtain different heat inputs

Sample designation	Current (A)	Voltage (V)	Speed (mm/min)	Heat input (J/mm)
A	70	12.2	235	175
B	80	12.4	255	185
C	90	12.5	275	195
D	100	12.9	305	205

recorded values were then used in the Eq. 1 to determine the heat input (J mm^{-1}) precisely.

$$\text{Heat Input, } Q = \frac{\eta \times V \times I \times 60}{S \times 1000} \quad (1)$$

where V = arc voltage in Volts, I = arc current in Amps, S = welding speed in mm/min and arc efficiency, $\eta = 0.8$

Metallographic specimens of weld cross-section were cut and the specimens were polished. Solution made of (70 ml Picral + 10 ml H_2O_2 + 10 ml Glacial Acetic acid) was used to etch the metallographic specimens to reveal the general microstructure of the joints. The metallographic specimens were observed by optical microscopy (OM) and scanning electron microscopy (SEM). A slice of specimen was also cut from the weld zone, diffusion layer and then thinned by ion beam milling to be observed by a transmission electron microscopy (TEM) with energy dispersive spectroscopy (EDS). The micro hardness distribution was measured by Wilson Wolpert micro-hardness tester with a load of 0.5 kg at regular interval for 15 s. Lap shear tensile test samples were also cut out from the resulted Al–Mg joints. The specimens were pulled by INSTRON 3367 30 kN testing machine with a constant loading rate of 0.5 mm/min.

Since residual stresses contributed to the weldments strength and corrosion resistance, it was therefore obligatory to have an idea about their relationship. The stresses were measured according by $\text{Sin}^2\psi$ method using Cr- $\text{K}\alpha$ radiation in a RIGAKU X-ray diffractometer equipped with a beam size of 1.5 mm \times 1.5 mm at 18 mA and 30 kV with a step size of 0.1 and 1 mm spot size. The diffracted rays were measured at different angles (Tilt angle, $\psi = 0\text{--}40$) by fixing a diffraction plane of {222} for Al alloys. Lattice constant of $\text{\AA} = 4.049$, Poisson's ratio of 0.322 and diffraction constant of 68.89 GPa were taken. Approximately 10 points were measured on the weld and 15 points on either sides.

To study the pitting corrosion behaviour, potentiodynamic polarization tests were carried out using a software based electrochemical system (Gill AC-1339, ACM instruments, UK). Experiments were carried out in aerated 3.5 % Sodium Chloride solutions with pH adjusted to 10 by adding potassium hydroxide. The exposure area for these experiments was 1 cm^2 . Potentials at which current

increased considerably was considered to be the critical pitting corrosion E_{pit} . Samples exhibiting relatively less negative or more positive potentials were considered to have higher pitting corrosion resistance. Tests were carried out according to the procedures laid in ASTM G-59. Comparison of variation in microstructure of the weld, fusion line, tensile strength, residual stress and corrosion behavior was made and correlated for all the designated heat inputs.

3 Results and Discussion

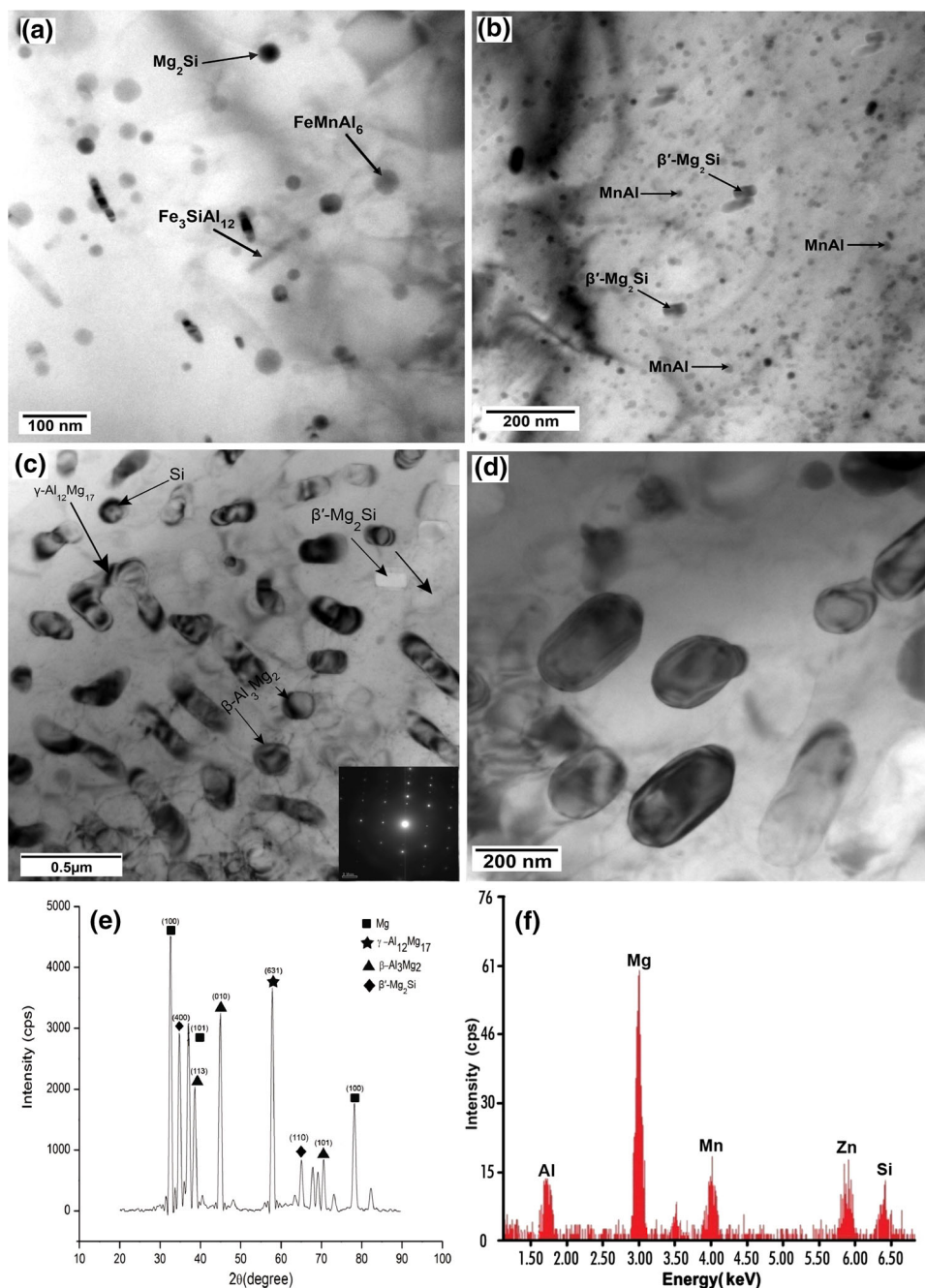
3.1 Microstructures of Base Metal and Weld Zone

TEM microstructure of the A6061-T6 alloy matrix with spherical eutectic particles of Mg_2Si (black rounded), $(\text{FeMn})\text{Al}_6$ (dark grey) and $\text{Fe}_3\text{SiAl}_{12}$ (script like) which appears as fine particles. These particles are further fragmented and uniformly distributed. Figure 2b shows the TEM micrograph of the AZ31B Magnesium consisting of outlined MnAl compound and with uniformly distributed Mg_2Si .

A homogeneous distribution of particles in the weld metal can be seen from (Fig. 2c) with filler containing rod like Al_6Mn particle (200 nm) with finely dispersed β' - Mg_2Si (50 nm). The existence of AlMn may be due to the low diffusion rate of Mn which requires more time to dissolve into the matrix [17]. Figure 2c shows that intermetallic β' - Mg_2Si particles are present along with Si particles. β - Al_3Mg_2 intermetallic appears in the form of quasi-spherical particles. Selected area electron diffraction (SAED) from these particles results in a hexagonal pattern. EDS analyses of these fine particles show that they contain Mg, Al, Si and Mn as shown in Fig. 2f. Presence of Mg_2Si , γ - $\text{Al}_{12}\text{Mg}_{17}$ and β - Al_3Mg_2 phase is evident from the XRD analysis as shown in Fig. 2e.

Macrostructure of A6061-T6 and AZ31B in the lap configuration is shown in Fig. 3a, b. The macrostructure shows perfect fusion between the materials with equal leg lengths. The welds are also free from process induced defects such as porosity and lack of fusion. Figure 3c–f shows the SEM-BSE image of the fusion line (diffusion layer) at the designated heat inputs. Thickness of the diffusion layer varies from 3 to 12 μm . The white spots are identified as Mg_2Si and black particles are MnAl compound. It is found that as the heat input increases, the layer thickness increases correspondingly. The solidification starts from the fusion line and ends at weld centre. When the weld solidifies, there will be significant contraction in the fusion line. This will be resisted and pulled back. Hence the fusion line exhibits wavy nature. It is also evident from the SEM that at low heat input of 175 J/mm, MnAl

Fig. 2 Bright Field-Transmission electron micrographs of base metals **a** Aluminum A6061-T6, **b** AZ31B Magnesium alloy with outlined MnAl compound, **c** Bright field image of the weld zone with Al_6Mn and $\beta\text{-Al}_3\text{Mg}_2$ phase, **d** Intermetallic $\beta'\text{-Mg}_2\text{Si}$ particles present along with $\beta\text{-Al}_3\text{Mg}_2$ phase, **e** XRD analysis on the weld revealing the presence of $\beta'\text{-Mg}_2\text{Si}$, $\gamma\text{-Al}_{12}\text{Mg}_{17}$ and $\beta\text{-Al}_3\text{Mg}_2$ phase, **f** EDS pattern showing the presence of Mg, Si, Al and Mn



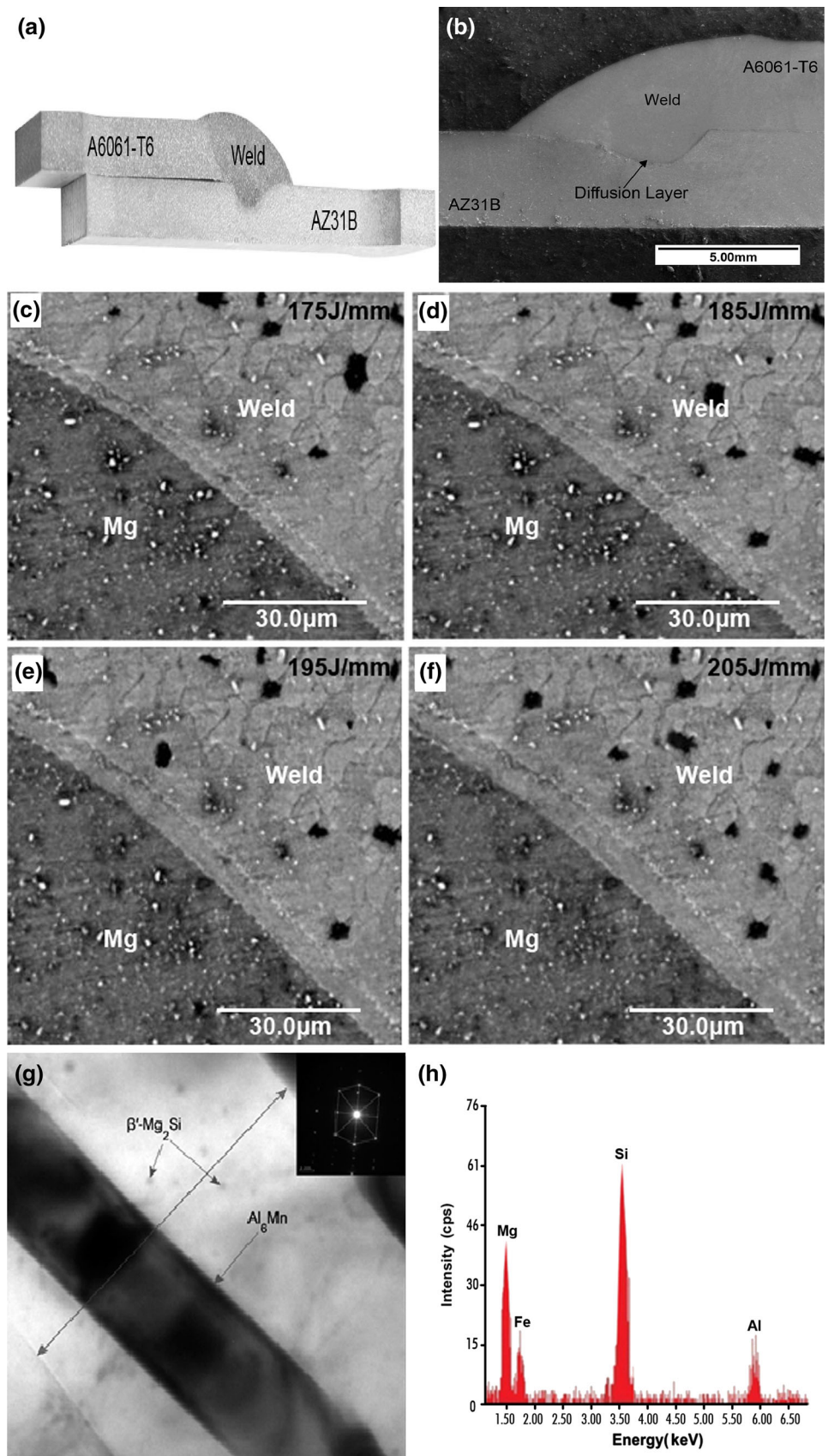
compound appears coarser with fine Mg_2Si particles. As the heat input increases, volume of Mg_2Si increases with MnAl becoming finer, uniformly distributed and present exactly at the dendritic boundaries. It is understood that presence of MnAl along with Mg_2Si enhances the joint strength considerably. TEM-EDS analysis on the IM compounds have a chemical composition of Al 68.86 %, Mn 29.35 %, Si 1.79 % which reveals that the particular spot is made of Al_6Mn with $\beta'\text{-Mg}_2\text{Si}$ dispersed therein (Fig. 3h). EDS spectrum also proves that there is some mutual interdiffusion during welding. It can be understood that Al_6Mn has formed first, during the chemical reaction

because of its morphology. Furthermore, according to the Scheil's solidification model, Al_6Mn forms first, followed by Mg_2Si . There is a good agreement for the above mentioned phenomena as several Mg_2Si grains are linked to a single Al_6Mn crystal. So it can be established that Mg_2Si and Al_6Mn are present in the diffusion layer.

3.2 Effect of Heat Input on the Hardness and Tensile Strength of the Dissimilar Welds

The micro hardness measured at different heat input at different locations on the sample is shown in (Fig. 4). At

Fig. 3 **a** Macrograph showing the entire weld cross section, **b** SEM micrograph showing the entire weld cross section, SEM-back scattered electron micrograph of the fusion line at **c** heat input 175 J/mm, **d** heat input 185 J/mm, **e** heat input 195 J/mm, **f** heat input 205 J/mm, **g** TEM micrograph showing intermetallic β' -Mg₂Si particles present along with Al₆Mn and spherical Si particles, **h** TEM-EDS pattern showing the presence of Al, Si, Fe and Mg



heat input of 185 J/mm the fusion region shows reduction in hardness due to coarsening of precipitates and coarser dendrites. The formation of coarser dendrites may be due to lower rate of cooling due to reduced welding speed. There is a slight increase in hardness at weld zone due to existence of alloying elements in solution condition. All the heat inputs fusion zone near magnesium show a higher hardness due to diffusion of alloying elements, formation of intermetallic compounds and existence of Mg_2Si and Al_6Mn precipitates. Joints produced at heat input of 205 J/mm has higher overall hardness at both the fusion zone as well as the weld because of increased welding speed and rapid solidification. This rapid solidification results in reduced micro segregation and the average pore size decreases as the cooling rate increases [19]. Due to rapid cooling rates, the dendrite arm spacing reduces and pore growth is thus limited. When dendrites are formed, those

regions do not have uniform density. The density is lower between the dendritic arms. As the solidification rate increases, the spacing between the dendritic arms (branches) decreases. This ensures that the region become more uniform in density, i.e., the porosity (the regions between the dendrites) is reduced. Due to rapid solidification, the quantity of hydrogen diffused into the weld pool is cut down drastically. This is because, when the cooling rate is increased, the solidification time is reduced. Diffusion is a time-dependent process. If the time is less then the quantity of hydrogen diffusing in will be less. And the hydrogen present in the solidified weld metal will also be less. Diffusion depends directly on diffusivity, the chemical potential and time (Fick's law). Hence, the weld metal porosity is reduced to a greater extent. Joints produced at heat input of 205 J/mm has the highest hardness compared to other heat inputs.

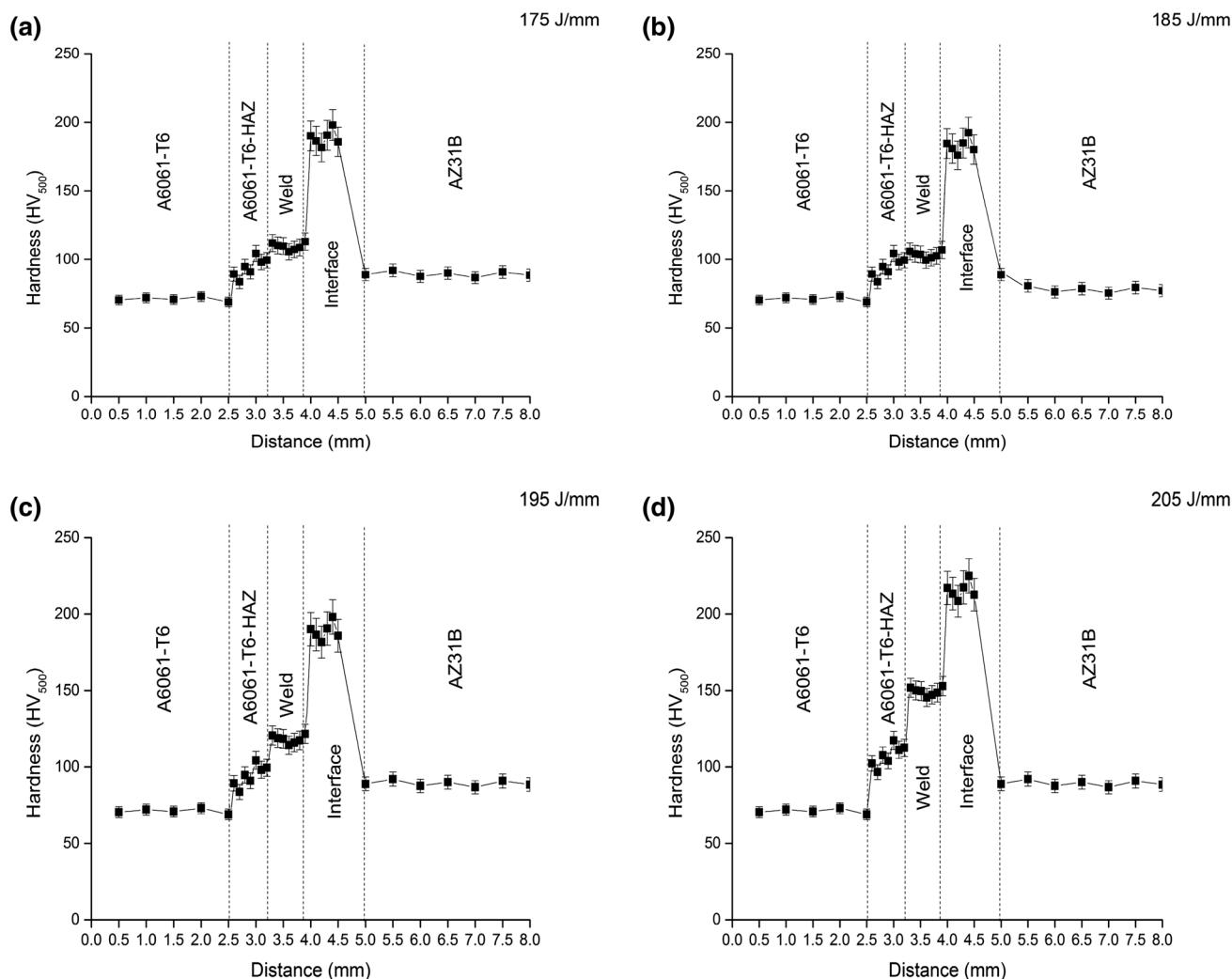


Fig. 4 Distribution of hardness along the cross sections of A6061-T6-AZ31B welds produced at **a** heat input 175 J/mm, **b** heat input 185 J/mm, **c** heat input 195 J/mm, **d** heat input 205 J/mm

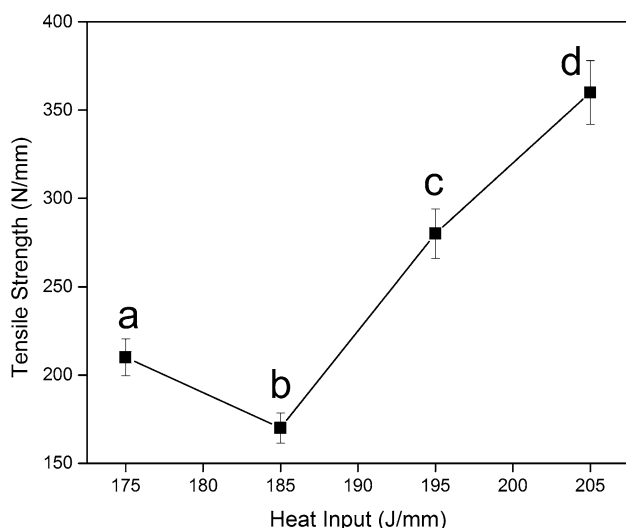


Fig. 5 Variation of tensile strength at the designated heat inputs of a 175 J/mm, b 185 J/mm, c 195 J/mm, d 205 J/mm

The tensile shear strength of A6061-T6-AZ31B Mg alloy joints obtained with different welding heat inputs are listed in Fig. 5. The joint made with heat input of 205 J/mm has the highest tensile strength. When the heat input is lower, traces of aluminium base metal dissolves into the weld metal, thereby the amount of strengthening phase dissolving into the weld is also reduced. The fusion zone softening primarily determines the joint tensile strength. Increase in heat input leads to greater softening and results in enhancing the tensile strength of the joints by increasing the diffusion layer thickness. With increase in the layer thickness, the volume fraction of Mg_2Si and $MnAl$ increases which also contribute to the enhanced joint strength. The melting points of Aluminum and Magnesium are 660 and 650 °C, respectively. Due to this small difference, restraining the formation of intermetallic compounds is difficult. But it can be controlled effectively by proper control over the heat input. Therefore, the heat input has significant effect on the mechanical strength of the joints. Hence suitable heat input must be determined not only to control the formation of intermetallic compounds but also to improve the joint strength [21].

3.3 Effect of Heat Input on Residual Stress

Figure 6 shows the measured transverse residual stress on the surface of the welds at different heat inputs. These stresses manifest due to restraints, thermal mismatch, phase transformation and localized strain [20]. It is evident that residual stresses also depend on the heat input. For the heat input (A = 185 J mm^{-1}), the tensile stress in the weld is the maximum. For heat input (D = 205 J mm^{-1}) the tensile stresses are at the minimum which results in high

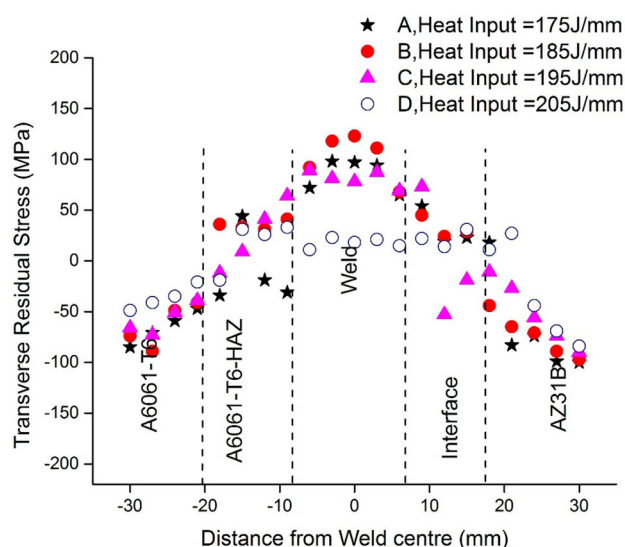


Fig. 6 Residual stress distribution across the Al–Mg dissimilar weld

tensile strength. This is because, as the heat input increases, heat percolates down to the interior more than when the heat input is less. Then, the difference between the rate of cooling of the top and lower layers will be less and so the tensile stress will also be less. The stress will be tensile because the top layer cools more than the lower layer and more of the contracting top layer will be pulled out. Tensile residual stress reduces with increasing heat input because of higher rise in temperature; because higher heat input will supply more energy to the weld pool and so the rate of solidification is supposed to be less. When there is no phase transformation, a slower cooling rate will lead to more uniform contraction of the sample from surface to the interior. Therefore, the tensile residual stress will be less.

3.4 Effect of Heat Input on Pitting Corrosion

The pitting corrosion potential variation with heat input is presented in Table 3. Relatively more positive potential values are obtained with increase in heat input. More positive potential value is an indication of better and improved pitting corrosion resistance (Fig. 7). It is clear from the microstructural study that fusion thickness increases with heat input. SEM studies also reveals that with increase in heat input, volume of Mg_2Si increases with $MnAl$ becoming finer and present exactly at the dendritic boundaries. Pitting corrosion occurs due to potential difference between intermetallics and the surrounding matrix. Observed improvement in pitting corrosion resistance with increase in heat input may be attributed to relatively higher cathodic nature of the precipitates. Compressive residual stress also assists in delaying the formation of pits and improves the pitting corrosion resistance. Hence improved

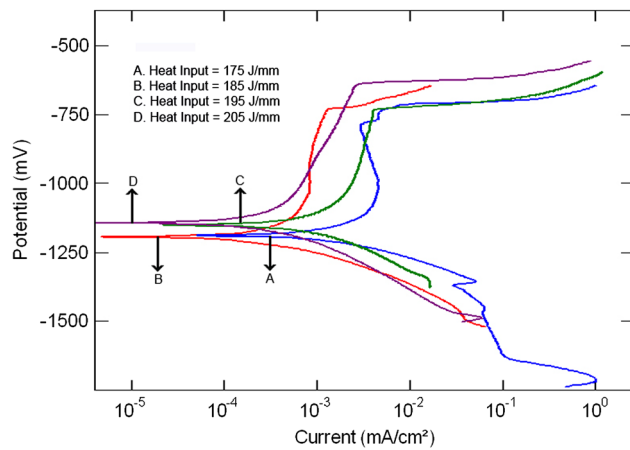


Fig. 7 Potentio-dynamic polarization curves at heat inputs of a 175 J/mm, b 185 J/mm, c 195 J/mm, d 205 J/mm

Table 3 Pitting corrosion potential (mV) of the weld zone at different heat inputs

Heat input designation	Heat input (J/mm)	Pitting corrosion potential, E_{pit} (mV)
A	175	-733
B	185	-794
C	195	-730
D	205	-643

pitting corrosion resistance of welds made with high heat input may also be due to minimal tensile residual stress.

4 Conclusions

Dissimilar welding between A6061-T6 aluminum alloy and AZ31B Magnesium alloy were made by CMT welding at different heat inputs. Microstructure and mechanical properties of the joints were evaluated and following conclusions have been reached.

- (1) Maximum tensile strength of 360 N/mm was achieved at a heat input of 205 J/mm. At higher heat inputs, tensile strength increased due to high welding speeds which resulted in minimal HAZ.
- (2) Thickness of the fusion line increased linearly from 3 to 12 μm with increase in the heat input. The thickness had significant effect on the joint strength. Electron microscopy analysis revealed that interfacial layer was composed of Mg_2Si and Al_6Mn phases.
- (3) Residual stresses were tensile in nature in the weld. Residual stresses also depended on the heat input. Increase in tensile strength was attributed to minimal tensile stress and finer precipitates.

- (4) Pitting corrosion resistance of lap welds was found to be better for higher heat input and might be attributed to the formation of intermetallic compounds of Mg_2Si and Al_6Mn in the interfacial layer which were relatively more cathodic.
- (5) A relationship between heat input, joint strength, residual stress and corrosion rate was established from this study. As the heat input increased, the corrosion resistance increased thereby increasing the joint strength. This was because, as the heat input increased, heat percolated down to the interior more than when the heat input was less. Then, the difference between the rate of cooling of the top and the bottom layers would be less resulting in a lower tensile stress. (The stress would be tensile because the top layer cooled more than the bottom layer and so due to higher contraction, the top layer would be pulled out). Lower the tensile stress, the crack propagation would be slower (stress corrosion cracking) and as the strength of a weld was directly proportional to the fracture stress, there was a direct relation between the corrosion resistance and the weld strength.

References

1. Kulekci M K, *Int J Adv Manuf Technol* **39** (2007) 851.
2. Schubert E, Klassen M, Zerner I, Walz C, and Sepold G, *J Mater Process Technol* **115** (2001) 2.
3. Chen Y C, and Nakata K, *Scripta Mater* **58** (2008) 433.
4. Zhang Z D, and Zhang F, *Mater Trans* **50** (2009) 1909.
5. Quan Y, Chen Z, Gong X, and Yu Z, *Mater Sci Eng A* **496** (2008) 45.
6. Qi X, and Song G, *Mater Des* **31** (2010) 605.
7. Hao X, and Song G, *IEEE Trans Plasma Sci* **37** (2009) 76.
8. Afrin N, Chen D L, Cao X, and Jahazi M, *Mater Sci Eng A* **472** (2008) 179.
9. Chi C T, Chao C G, Liu T F, and Wang C C, *Mater Sci Eng A* **435** (2008) 672.
10. Borrisutthekul R, Miyashita Y, and Mutoh Y, *Sci Technol Adv Mater* **6** (2005) 199.
11. Kwon Y J, Shigematsu I, and Saito N, *Mater Lett* **62** (2008) 3827.
12. Mahendran G, Balasubramanian V, and Senthilvelan T, *Mater Des* **30** (2009) 1240.
13. Kore S D, Imbert J, Worswick M J, and Zhou Y, *Sci Technol Weld Join* **14** (2009) 549.
14. Durgutlu A, Gulenc B, and Findik F, *Mater Des* **26** (2005) 497.
15. Honarpisheh M, Asemabadi M, and Sedighi M, *Mater Des* **37** (2012) 122.
16. Pourahmad P and Abbasi M, *Trans Nonferrous Met Soc China* **23** (2013) 1253.
17. Shen J, Li Y, Zhang T, Peng D, Wang D, and Xu N, *Sci Technol Weld Join* **20** (2015) 1.
18. Elrefaey A, *Sci Technol Weld Join* **20** (2015) 280.
19. Sun C Y, and Mondolfo L F, *J Inst of Met* **95** (1967) 384.
20. Francis J A, Bhadeshia H K D H, and Withers P J, *Mater Sci Technol* **23** (2007) 1009.
21. Poorhaydari K, Patchett B M, and Ivey D G, *Weld J* **84** (2005) 149.